Mycelium-Coir-Based Composites for Sustainable Building Insulation

Gargi De[1,2#], Libin Yang[1,2#], Jaejun Lee[3], Yu-Han Wu[3], Zhiting Tian[4], Zhao Qin[1,2,5]*

[1] Laboratory for Multiscale Material Modelling, Syracuse University, 151L Link Hall, Syracuse University, Syracuse, NY 13244, USA

[2] Department of Civil and Environmental Engineering, Syracuse University, 151L Link Hall, Syracuse University, Syracuse, NY 13244, USA

[3] Department of Materials Science and Engineering, Cornell University, Ithaca, New York, 1483. USA

[4] Sibley School of Mechanical and Aerospace Engineering, Cornell University, Ithaca, NY 14853, USA

[5] The BioInspired Institute, Syracuse University, NY 13244, USA

# These authors contribute equally to the work

*Materials & Correspondence should be addressed to Z.Q. (zqin02@syr.edu)

Supplementary Information

Supplementary Experimental Methods

The thermal conductivity and density of different MBCs: Data is obtained from different literatures [1,2,11–20,3,21–27,4–10].

Differential Scanning Calorimetry for heat capacity: TA Instruments Differential Scanning Calorimeter (DSC) Auto 2500 is used for heat capacity measurements. DSC involves a single furnace where the sample and reference undergo a controlled heat-cool-heat cycle. Approximately 2–3mg of the sample, placed in an aluminum pan, and an empty reference pan are positioned on a thermoelectric disk within the furnace. Heat is transferred to the sample and the reference as the furnace temperature changes at a constant rate of 10°C per minute. Area thermocouples measure the differential heat flow. The heat flow amplitude comprises a heat capacity component and a kinetic component.

Compression Test: Compression tests were performed on each 50·50·50 mm^3 brick sample using an Instron 5966 machine (10 kN static load cell) to obtain stress-strain curves in tension. We measure the initial sample length as the distance between the edges of the two plates as L_0 before the test. During our tests, the lower plate is fixed, and the upper plate moves at a constant displacement speed of $v = -$ 2mm/min. The traveling distance of the upper plate is given by d at any time after the test starts, updated every 0.02 seconds, and the engineering strain of the sample is defined by $\varepsilon = d/L_0$. The load cell records the loading force F and computes the engineering stress with $\sigma = F/A_0$, where A_0 is the initial middle part cross-section area of the testing region of

the brick sample. We use the $\varepsilon - \sigma$ data from $\varepsilon = 0$ to $\varepsilon = 0.002$ to perform the linear fitting and measure the slope of the fitting curve to calculate Young's modulus (*E*). We use the equation of $\sigma = E\varepsilon$ to draw the linear function. The intersection between the linear function and the $\varepsilon - \sigma$ curve is the 0.2% yield stress. We measure the area under the entire $\varepsilon - \sigma$ curve to obtain the toughness modulus (U).

Dog bone sample by heat press and tensile test: The press machine connected with the Proportional-Integral-Derivative (PID) temperature controller box allows us to set constant temperatures (*T*). A two-part aluminum mold is used to make the MBC sample of a type-IV dog-bone shape according to ASTM D638 standard. The former work of data-driven model and its predictions of the most promising treatment conditions (*i.e.*, temperature *T*, pressure *P* and treatment time *t* as shown in **Fig. S4A**) that yields maximum specific strength (*i.e.*, OS for *T*=88°C, *P*=28.11 MPa and *t*=9.8 hours) and maximum specific toughness (*i.e.*, OT for *T*=91 °C, *P*=22.69 MPa and *t*=7.5 hours) in tensile loading are adopted to test material samples before tensile tests. To validate their effectiveness, we modified these optimal conditions by increasing and decreasing the total treatment time (OSt-50, OTt-50, and OSt+50, OTt+50, respectively) by 50%, as well as by increasing and decreasing the pressure during the treatment period (OSp-50, OTp-50 and OSp+50, OTp+50, respectively, see detailed conditions in **Table S4**). We did not change the temperature because the optimal treatment condition of 90°C can effectively dry the samples without degrading the mycelium fibers. Heat pressing is employed to enhance the alignment and packing density of fibers in the composite, as observed in previous studies on bacterial cellulose films, where the process significantly improved the mechanical properties by facilitating strong hydrogen bonding between aligned nanofibrils.[28] This effect increases the tensile strength and toughness of the material, as the densification and enhanced alignment achieved during pressing contribute to better load transfer and structural integrity. For each sample, when the temperature of the hot plates reaches the desired one, we put the mold with material and compress it with a 10-ton heat press machine with the hydraulic hand pump under constant pressure (*P*) on the sample, as shown in **Fig. S2**. We allow the heat-presser to bake the sample until the targeted time (*t*). We perform tensile tests on each dog-bone sample with the Instron machine (10 kN static load cell, 1 kN pneumatic grips with 90 psi (0.62 MPa) holding pressure) to obtain its stress-strain curves in tension. The lower grips are fixed, and the upper grips move at a constant displacement speed of $v = 0.5$mm/min during our tests. The traveling distance of the upper grips is given by d at any time after the test starts, updated for every 0.02 seconds. The test automatically stops when the sample is broken in tension. We measure the maximum stress of the entire $\varepsilon - \sigma$ curve as the ultimate stress.

Supplementary Tables

Table S1. List of MCBC samples, the parameters during their preparation and sample names. As well as their mechanical properties are obtained from compression tests.

Growth Period	Forming Mold Shape	Mycelium Culture Source	Nutrition Concentration	Sample Name	0.2% σ_c (MPa)	E (MPa)	U (J·m^{-3})
1 week	50 mm × 50 mm	liquid	160 g/L malt with 80 g/L yeast	SLS-1	0.55	2.88	0.799
				SLS-2	0.74	4.00	0.887
				SLS-3	0.73	3.66	0.888
			240 g/L malt with 120 g/L yeast	SLL-1	0.69	3.50	0.852
				SLL-2	0.73	3.85	0.895
				SLL-3	0.75	3.87	0.892
		rye	160 g/L malt with 80 g/L yeast	SRS-1	0.53	2.52	0.896
				SRS-2	0.52	2.54	0.908
				SRS-3	0.88	4.54	0.932
			240 g/L malt with 120 g/L yeast	SRL-1	0.83	4.16	0.940
				SRL-2	0.87	4.22	0.948
				SRL-3	0.89	4.66	0.931
2 weeks	150 mm × 150 mm	rye	160 g/L malt with 80 g/L yeast	LRS-1	0.81	3.96	0.995
				LRS-2	0.87	4.06	0.970
				LRS-3	0.60	2.85	0.980
			240 g/L malt with 120 g/L yeast	LRL-1	0.25	1.26	0.597
				LRL-2	0.35	1.63	0.627
				LRL-4	0.27	1.42	0.577
4 months	50 mm × 50 mm	rye	240 g/L malt with 120 g/L yeast	SRLL-1	0.12	0.56	0.413
				SRLL-2	0.10	0.62	0.545
				SRLL-3	0.08	0.44	0.646

Table S2. Comparative analysis of thermal resistance values (R-values), thickness, and specific thermal resistance for different building materials, including basswood, plywood, drywall, EPS board, mycelium board (SRLL sample), and pure mycelium (*G. lucidum*) film.

Material type	Thermal resistance (m^2·K/W)	R-value (Imperial) (ft^2·°F·h/BTU)	Thickness (m)	Specific thermal resistance (m·K/W)	Specific R-value (R-value/inch)	Thermal conductivity k (W·m^{-1}·K^{-1})
Basswood	0.29	1.67	0.013	23.10	3.33	0.043
Plywood	0.17	0.95	0.0064	26.49	3.82	0.038
Drywall	0.15	0.82	0.0064	22.84	3.29	0.044
EPS board	0.88	5.00	0.025	34.67	5.00	0.029
MCBC board	0.70	3.98	0.0203~ 0.0305	22.97~ 34.45	3.31~ 4.97	0.029~0.044
Pure MF	0.0034	0.020	0.000047	72.57	10.47	0.015

G. lucidum						

Sample	Average Diffusivity ($m^2 \cdot s^{-1}$)	Mass (kg)	Thickness (m)	Density ($kg \cdot m^{-3}$)	Specific heat capacity ($J \cdot kg^{-1} \cdot K^{-1}$)	Thermal Conductivity ($W \cdot m^{-1} \cdot K^{-1}$)
P.E.	1.87.E-08	5.50E-06	5.02E-05	865	1111	0.019 ± 0.0036
GL	2.39.E-08	4.20E-06	4.74E-05	699	825	0.015 ± 0.0033
T.V	1.59.E-08	3.80E-06	2.27E-05	1321	855	0.027 ± 0.018
F.V	6.91.E-08	5.30E-06	4.93E-05	849	973	0.059 ± 0.011
P.O	2.46.E-08	7.10E-06	9.40E-05	596	1055	0.016 ± 0.0032
G.S	5.75.E-08	4.30E-06	7.66E-05	443	851	0.023 ± 0.0044

Table S3. The physical properties of MF samples correspond to different mycelium species

Table S4. Thermal conductivity and density of MCBC compared to other bio-based insulation materials

Material	Density ($kg \cdot m^{-3}$)	Thermal Conductivity ($W \cdot m^{-1} \cdot K^{-1}$)	Source
MCBC	170	0.035 ± 0.008	Current Study
Eucalyptus Fiber Bark Panels (EGFB)	80 to 300 (target density)	0.064 – 0.077	Fuentealba et al., 2024[29]
Coconut Palm Fibre Panels	-	0.40 (average)	Mededji et al., 2024[30]
Eelgrass	120	0.05*	Ranefjärd et al., 2024[31]
Grass	40	0.041*	Ranefjärd et al., 2024[31]
Wood Fibre	50	0.038*	Ranefjärd et al., 2024[31]
Flexible Hemp Batt (FHB)	34	~0.04	Lafond et al., 2020[32]
Hemp Fibers + Cellulose fibers in the ratio of 60:40	30 - 60	0.046	Reif et al., 2016[33]
Cellulose Fibers 100%	30 - 60	0.039 – 0.042	Reif et al., 2016[33]
Cellulose Fibers + Straw in the ratio of 30:70	30 - 60	0.040 – 0.042	Reif et al., 2016[33]
Straw 100%	95 - 120	0.045 – 0.046	Reif et al., 2016[33]

*Manufacturer values, values measured by authors were slightly higher.

Table S5. Mechanical properties and density of different densified MCBC samples after heat-press treatment under the combination of temperature (*T*), pressure (*P*) and treatment time (*t*). The mechanical properties are obtained from tensile tests.

Treatment Name	*T* (°C)	*P* (MPa)	*t* (hours)	ρ (g·cm^{-3})	σ_u (MPa)	E (MPa)	U (MJ·m^{-3})
OS	88	28.11	9.8	1.42	12.47	3200.5	0.043
				1.37	12.45	2268.7	0.050
				1.35	10.99	2314.9	0.052
OT	91	22.69	7.5	1.48	10.60	2624.9	0.066
				1.50	10.63	2560.3	0.037
				1.42	10.93	2711.4	0.074
OSt-50	88	28.11	4.9	1.45	9.66	2685.4	0.032
				1.33	9.58	2335.3	0.036
				1.32	9.37	2114.0	0.062
OTt-50	91	22.69	3.75	1.31	6.24	1399.7	0.030
				1.32	6.36	1615.5	0.030
				1.27	6.90	1876.1	0.044
OSt+50	88	28.11	14.7	1.47	8.06	2189.7	0.039
				1.38	8.06	2062.0	0.030
				1.44	8.39	2345.5	0.024
OTt+50	91	22.69	11.25	1.40	4.40	1324.1	0.017
				1.47	4.73	1466.2	0.045
				1.42	4.31	1343.9	0.016
OSp-50	88	14.05	9.8	1.51	7.29	2699.1	0.015
				1.35	7.38	1782.5	0.043
				1.38	7.72	2117.0	0.037
OTp-50	91	11.35	7.5	1.21	3.61	1308.8	0.023
				1.11	3.86	1487.9	0.027
				1.38	3.76	1458.4	0.015
OSp+50	88	42.17	9.8	1.39	9.33	2164.5	0.049
				1.46	10.09	2346.4	0.042
				1.41	9.98	2553.9	0.029

ОТр+50	91	34.04	7.5	1.40	5.61	1513.1	0.019
				1.46	5.82	1660.5	0.035
				1.38	5.84	1444.2	0.050

Supplementary Figures

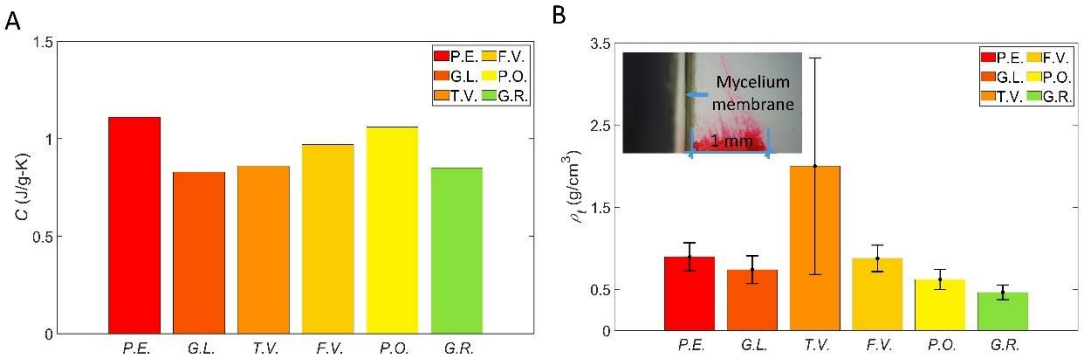

Figure S1. A. DSC measurement of the thermal capacity of MF samples. **B.** Average density and deviation of MF samples. The inserted microscope image gives an example of the cross-section and thickness measurement.

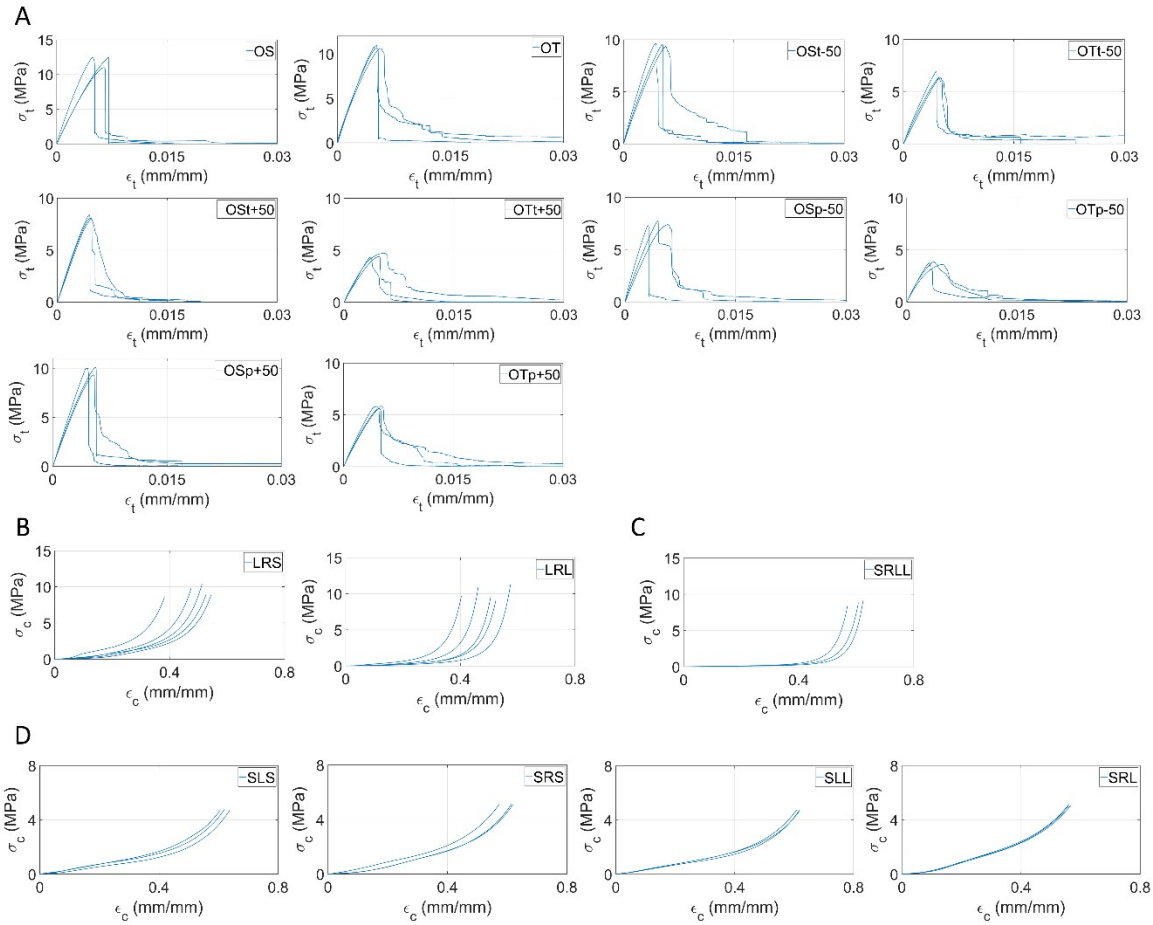

Figure S2. A. Stress-strain curves for various dog bone shape samples under different treatment conditions. The treatments include the original specific ultimate stress (OS), the original specific toughness (OT) with a baking time increase and decrease of 50% (t+50 and t-50), and pressure increase and decrease of 50% (p+50 and p-50). Showing how the different treatment conditions affect the mechanical behavior of the materials. **B.** Stress-strain curves for mycelium-based bio-composite bricks are prepared by inoculating coir by using rye mycelium culture and 2 different amounts of nutrition concentrations in the larger square mold for 2 weeks. (L: larger mold, R: rye mycelium culture, S: low nutrition concentration, and L: high nutrition concentration). **C.** Stress-strain curves for mycelium-based bio-composite bricks that are prepared by inoculating coir using rye mycelium culture and a concentration of nutrition in the small square mold for 4 months. (S: small mold, R: rye mycelium culture, L: high nutrition concentration, and L: longest growth time). **D.** Stress-strain curves for mycelium-based bio-composite bricks that are prepared by inoculating coir by using 2 different mycelium cultures and 2 different amounts of nutrition concentrations in the small square mold for 1 week. (S: small mold, R: rye mycelium culture, L: liquid mycelium culture, S: low nutrition concentration, and L: high nutrition concentration). B, C, and D show how the different growth periods, forming mold shape, mycelium culture source, and nutrition concentration affect the mechanical behavior of the materials.

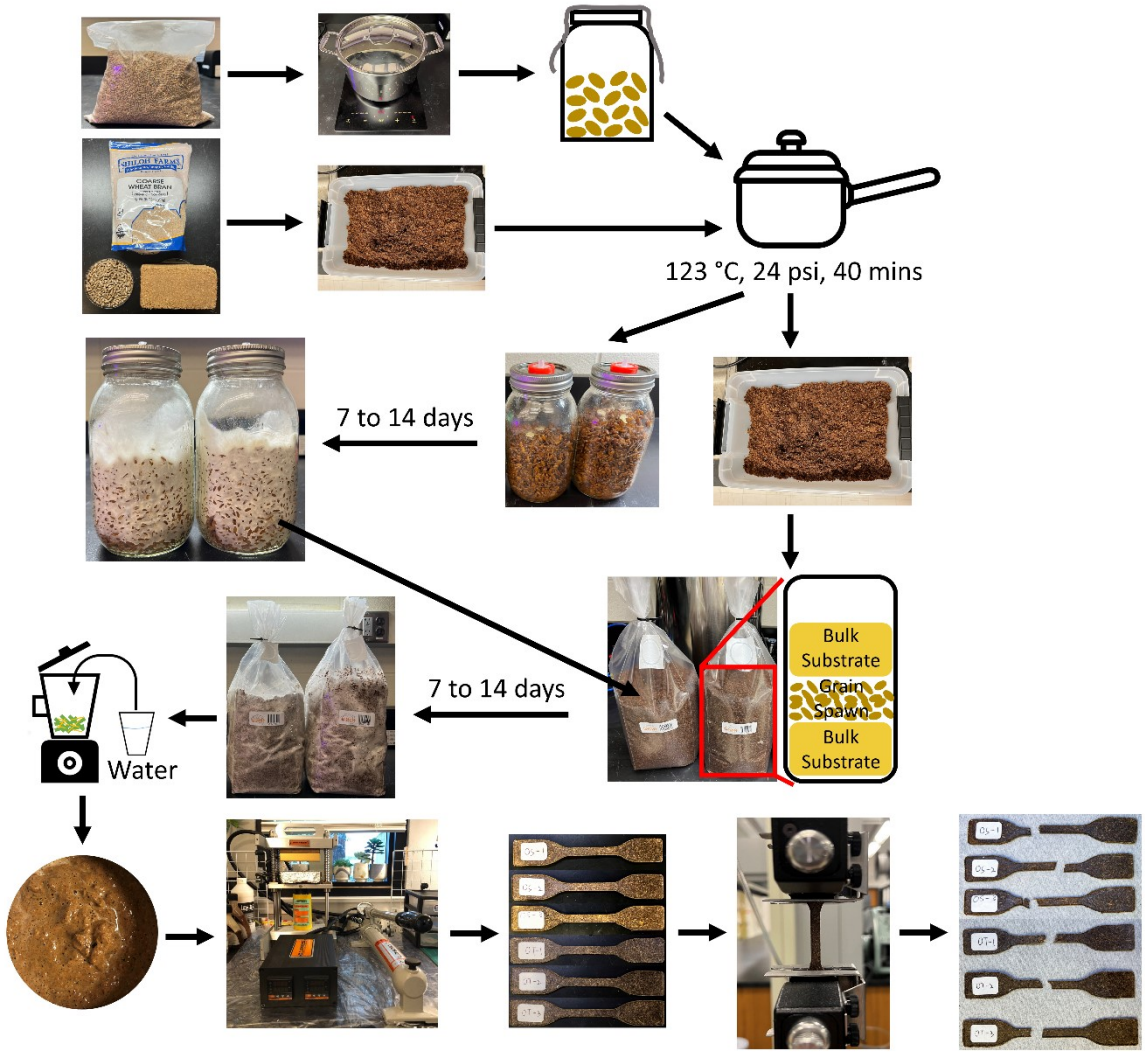

Figure S3. The general process of making dog bone shape samples. Preparing the rye mycelium culture first, then inoculating it with the composite material to make the mycelium-based bio-composite bag for making the food bone shape samples. The dog bone samples shown in the figure are made with coir and oak wood with wheat as the nutrition based on different treatment conditions (material/mixed with water / mushy material / heat-press machine/test samples / Instron machine / broken samples).

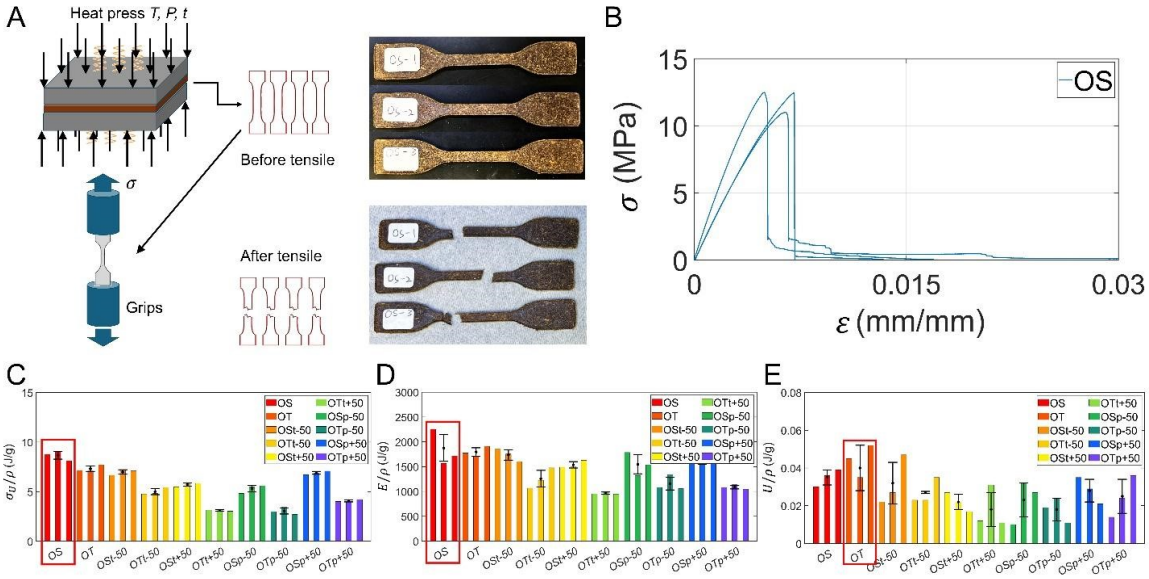

Figure S4. Heat press of MCBC for optimal tensile mechanics after densification. A. Schematics of the MCBC dog bone samples in heat press and tensile mechanical loading test, as well as densified MCBC samples after treatment under OS condition and their failure form after fracture in tensile loading. **B.** $\sigma - \varepsilon$ curves of OS samples in tensile tests, where specific mechanical properties, including **C.** ultimate stress ($^{\sigma_U}/_{\rho}$), **D.** Young's modulus (E/ρ), and **E.** toughness (U/ρ), are learned from the $\sigma - \varepsilon$ curves for samples obtained from OS, OT and other mutated (*e.g.*, OSt/p ± 50, OTt/p ± 50) treatment conditions as summarized in **Table S4** in the Supporting Information. It is shown that the treatment condition from the mechanical learning results (OS and OT conditions from [34]) gives us the maximum specific mechanical properties, suggesting that the mechanical learning results are accurate. Moreover, the variations in treatment conditions lead to worse mechanics, suggesting these treatment conditions have nonlinear effects on material mechanics, and the optimal treatment conditions (OS and OT) take the saddle point for the treatment-mechanics relationship.

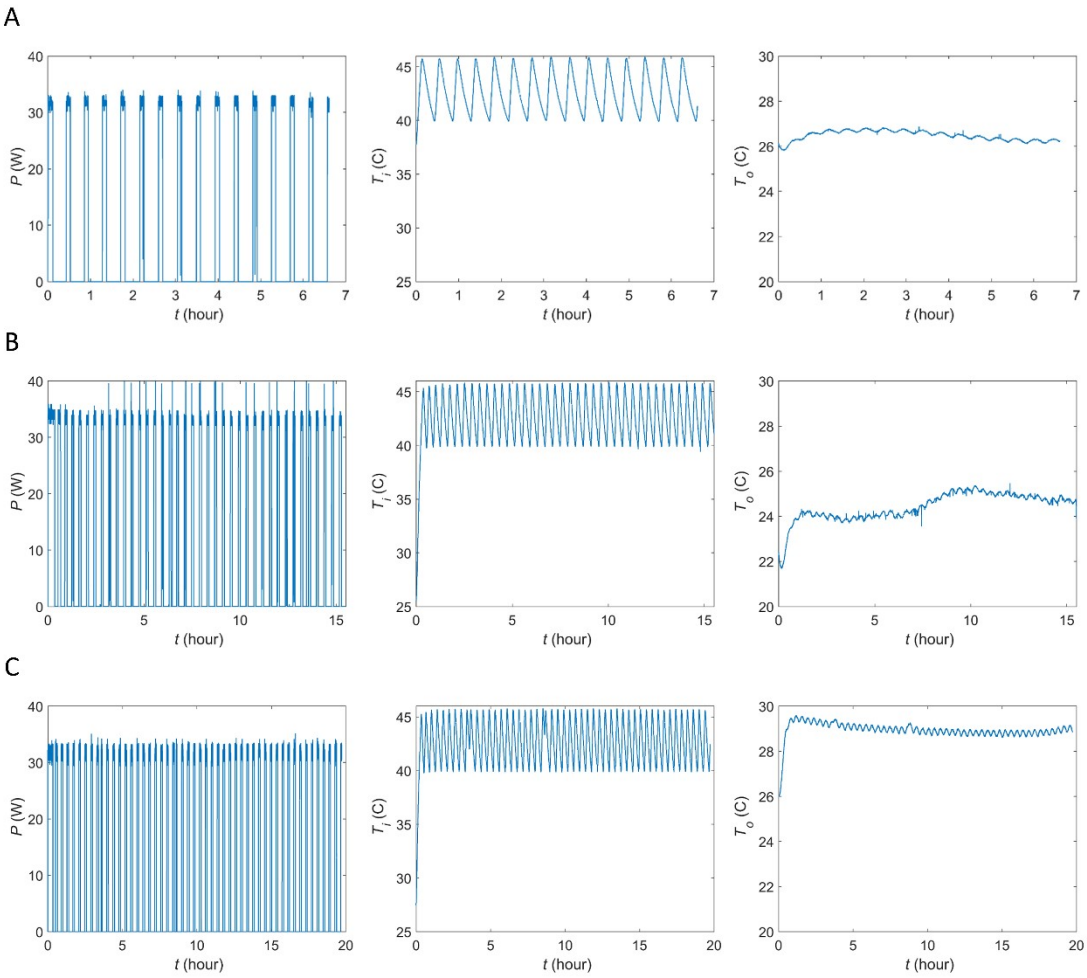

Figure S5. A. Heat-flux time curve, as well as the temperature inside and outside the chamber of the custom-built mid-size chamber for the original box after equilibration. **B.** Heat-flux-temperature -time curves for the custom-built mid-size chamber, with the top layer replaced by the sandwich structure of MCBC SRLL core plus the two 1/8-inch basswood surface panels. **C.** Heat-flux-temperature-time curves for the custom-built mid-size chamber, with the top layer replaced by stacking of four 1/8-inch basswood panels.

Supplementary References

[1] T. Vallas, L. Courard, *Front. Archit. Res.* **2017**, *6*, 318.

[2] E. César, M. A. Castillo-Campohermoso, A. S. Ledezma-Pérez, L. A. Villarreal-Cárdenas, L. Montoya, V. M. Bandala, A. M. Rodríguez-Hernández, *Biocatal. Agric. Biotechnol.* **2023**, *47*, 102602.

[3] J. Cai, J. Han, F. Ge, Y. Lin, J. Pan, A. Ren, *Constr. Build. Mater.* **2023**, *389*, 131730.

[4] F. Gauvin, V. Tsao, J. Vette, H. J. H. Brouwers, *Constr. Technol. Archit.* **2022**, *1*, 643.

[5] H. Schritt, S. Vidi, D. Pleissner, *J. Clean. Prod.* **2021**, *313*, 127910.

[6] P. P. Dias, L. B. Jayasinghe, D. Waldmann, *Results Mater.* **2021**, *10*, 100189.

[7] G. A. Holt, G. McIntyre, D. Flagg, E. Bayer, J. D. Wanjura, M. G. Pelletier, *J. Biobased Mater. Bioenergy* **2012**, *6*, 431.

[8] M. Früchtl, A. Senz, S. Sydow, J. B. Frank, A. Hohmann, S. Albrecht, M. Fischer, M. Holland, F. Wilhelm, H.-A. Christ, *Polymers (Basel).* **2023**, *15*, DOI 10.3390/polym15153205.

[9] P. Amstislavski, T. Pöhler, A. Valtonen, L. Wikström, A. Harlin, S. Salo, P. Jetsu, G. R. Szilvay, *Cellulose* **2024**, *31*, 8769.

[10] P. Jinanukul, J. Kumla, W. Aiduang, W. Thamjaree, R. Oranratmanee, U. Shummadtayar, Y. Tongtuam, S. Lumyong, N. Suwannarach, T. Waroonkun, *J. Fungi* **2024**, *10*, DOI 10.3390/jof10090634.

[11] M. Fellah, S. Ouhaibi, N. Belouaggadia, K. Mansouri, H. Naji, *Case Stud. Constr. Mater.* **2024**, *20*, e02786.

[12] C. H. Koh, F. Gauvin, K. Schollbach, H. J. H. Brouwers, *Constr. Build. Mater.* **2022**, *346*, 128440.

[13] X. Zhang, J. Hu, X. Fan, X. Yu, *J. Clean. Prod.* **2022**, *342*, 130784.

[14] F. Pittau, O. G. Carcassi, M. Servalli, S. Pellegrini, S. Claude, *IOP Conf. Ser. Earth Environ. Sci.* **2022**, *1078*, 12069.

[15] H. Mbabali, M. Lubwama, V. A. Yiga, E. Were, H. Kasedde, *J. Inst. Eng. Ser. D* **2024**, *105*, 97.

[16] Q. Jin, Z. Zhang, J. Chen, *J. Build. Eng.* **2024**, *92*, 109646.

[17] O. B. Carcassi, P. Minotti, G. Habert, I. Paoletti, S. Claude, F. Pittau, *Sustainability* **2022**, *14*, DOI 10.3390/su14031384.

[18] E. D. Gezer, S. Kuştaş, *BioResources* **2024**, *19*, 1348.

[19] A. Livne, H. A. B. Wösten, D. Pearlmutter, E. Gal, *ACS Sustain. Chem. Eng.* **2022**, *10*, 12099.

[20] A. Livne, D. Pearlmutter, E. Gal, H. A. B. Wösten, *Constr. Build. Mater.* **2024**, *421*, 135566.

[21] W. Sun, M. Tajvidi, C. G. Hunt, B. J. W. Cole, C. Howell, D. J. Gardner, J. Wang, *J.*

Clean. Prod. **2022**, *353*, 131659.

[22] E. Elsacker, S. Vandelook, J. Brancart, E. Peeters, L. De Laet, *PLoS One* **2019**, *14*, e0213954.

[23] M. Zhang, Z. Zhang, R. Zhang, Y. Peng, M. Wang, J. Cao, *Compos. Part B Eng.* **2023**, *266*, 111003.

[24] M. Zhang, J. Xue, R. Zhang, W. Zhang, Y. Peng, M. Wang, J. Cao, *Small* **2023**, *19*, 2302827.

[25] M. Nussbaumer, D. Van Opdenbosch, M. Engelhardt, H. Briesen, J. P. Benz, T. Karl, *Environ. Technol. Innov.* **2023**, *30*, 103063.

[26] C. Charpentier-Alfaro, J. Benavides-Hernández, M. Poggerini, A. Crisci, G. Mele, G. Della Rocca, G. Emiliani, A. Frascella, T. Torrigiani, S. Palanti, *Mater. (Basel, Switzerland)* **2023**, *16*, DOI 10.3390/ma16093547.

[27] Y. Z. (Joey), Z. Feng, S. Benjamin, W. Maria, A. Philippe, *J. Mater. Civ. Eng.* **2017**, *29*, 4017030.

[28] S. Wang, T. Li, C. Chen, W. Kong, S. Zhu, J. Dai, A. J. Diaz, E. Hitz, S. D. Solares, T. Li, L. Hu, *Adv. Funct. Mater.* **2018**, *28*, 1707491.

[29] C. Fuentealba, C. Segovia, M. Pradena-Miquel, A.G. César, *Forests* **2024**, *15*, 1628.

[30] D. S. Mededji, E. Sogbochi, A. A. Djossou, O. Cherkaoui, L. A. Fagbemi, D. C. K. Sohounhloue, *Int. J. Environ. Clim. Change* **2024**, *14*, 324.

[31] O. Ranefjärd, P. B. Strandberg-de Bruijn, L. Wadsö, *Mater.* **2024**, *17*, 2021.

[32] C. Lafond, P. Blanchet, *Buildings* **2020**, *10*, 81.

[33] M. Reif, J. Zach, J. Hroudová, *Procedia Eng.* **2016**, *151*, 368–374.

[34] L. Yang, Z. Qin, *Cell Reports Phys. Sci.* **2023**, *4*, 101424.